Deformation of olivine at 5GPa and 350-900 °C

Simon A. Hunt, David P. Dobson, Ian G. Wood, John P. Brodholt, Julian Mecklenburgh, Edward C. Oliver

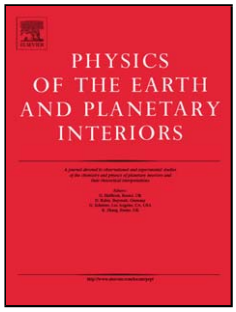

Title: Deformation of olivine at 5GPa and 350-900 °C

Authors: Simon A. Hunt, David P. Dobson, Ian G. Wood, John P. Brodholt, Julian Mecklenburgh, Edward C. Oliver

PII: S0031-9201(08)00111-8
DOI: doi:10.1016/j.pepi.2008.05.012
Reference: PEPI 4954

To appear in: *Physics of the Earth and Planetary Interiors*

Received date: 26-9-2007
Revised date: 21-4-2008
Accepted date: 29-5-2008

Please cite this article as: Hunt, S.A., Dobson, D.P., Wood, I.G., Brodholt, J.P., Mecklenburgh, J., Oliver, E.C., Deformation of olivine at 5GPa and 350-900 °C, *Physics of the Earth and Planetary Interiors* (2007), doi:10.1016/j.pepi.2008.05.012

PEPI_4954

Title:

Deformation of olivine at 5GPa and 350-900°C

Authors:

Simon A Hunt[1], David P Dobson[1], Ian G Wood[1], John P Brodholt[1], Julian Mecklenburgh[2], Edward C Oliver[3]

Affiliation:

1 Department of Earth Sciences, University College London, Gower Street, London WC1E6BT, UK
2 School of Earth, Atmospheric and Environmental Sciences, University of Manchester, Oxford Road, Manchester, M13 9PL, UK
3 ISIS Neutron Scattering Facility, Science and Technology Facilities Council, Rutherford Appleton Laboratory, Harwell Science and Innovation Campus, Didcot, OX11 0QX, UK

Knowledge of the rheology of the upper mantle is important for understanding both subduction related phenomena and mantle flow in general. Here we report the results of stress relaxation experiments on San Carlos olivine at pressures between 5.3 and 1.3 GPa and from 350 to 900^{o}C. At 5GPa and 500^{o}C the deformation best follows a model governed by long-range resistance to movement of dislocations. The yield stress of olivine has been measured at low strain rates of 10^{-7} s^{-1}. We conclude that the upper limit for the long term yield stress of olivine at 500^{o}C is 68 +180/-44 MPa.

We observe significant weakening and infer an associated change in deformation mechanism in olivine between 500 and 730^{o}C. This change is coincident with the limit of the seismogenic layer and the greatest elastic thickness measurements in oceanic crust.

Introduction

The Earth's upper mantle and subducting oceanic lithosphere are composed principally of olivine (α-$(Mg,Fe)_2SiO_4$) (e.g. Bina & Wood, 1986). Freed & Bürgmann (2004) estimated the rheology of the upper mantle using post-seismic deformation and concluded that upper mantle rheology is consistent with that of olivine. Therefore, the rheology of olivine is important for understanding the dynamics of the upper mantle and of subducting slabs.

Over longer time scales than those of post-seismic relaxation, the upper limit to the seismogenic (McKenzie *et al*., 2005) and elastic thicknesses (Watts, 2001) of the oceanic crust appears to be approximated by the 600^{o}C isotherm of McKenzie *et al*. (2005). Similarly, the cessation of intermediate seismicity corresponds closely with the 800^{o}C isotherm in subducting slabs (Frohlich, 2006). The concurrence of these measurements, which sample a large range of time scales and tectonic settings, indicates something about the fundamental properties of the material in which they occur, namely olivine.

Another proxy for the material properties of the upper mantle are the stress drops measured from intemediate and deep earthquakes. The stress drop observed during earthquakes shows an increasing trend with depth (Frolich, 1989; Venkataraman & Kanamori, 2004, and references therein); above 40km the typical stress drop observed is ≈ 1 to 10 MPa (Kanamori & Anderson, 1975). Between 50 and 100 km the stress drop rises to ≈ 11 to 42 MPa and at depths of 600 km stress drops of 16 to 280 MPa are observed.

Fundamental to this mechanical behaviour is the yield stress which, in a Bingham plastic fluid, is the stress required for the onset of plastic flow ‘under the conditions of the experiment’ (Scott Blair, 1933). Experimental measurement of the onset, or in a stress relaxation experiment the cessation, of flow is very difficult and so flow stresses are normally measured. The flow stress is the stress needed for flow at a given strain rate.

Despite the large body of work on the rheology of olivine, relatively few studies have attempted to determine its yield stress. Evans & Geotze (1979) used indentation techniques to show that the flow stress of olivine reduces with increasing temperature to 1500^{o}C and Green & Borch (1987) showed that it scales to the homologous temperature. The rheology of olivine has been studied at low pressure (<2 GPa) by

Ross *et al.* (1979) among others and, with the development of higher pressure techniques, at up to 10 GPa by Li *et al.* (2004), Raterron *et al.* (2004) and Yamamoto *et al.* (2008). These studies find that at high temperatures a power law rheology (equation 7) is observed while at lower temperatures (<700^{o}C) a short-range obstacle (Peierl's) plasticity is observed (equation 6a).

In this study the rheology of olivine has been investigated by stress relaxation experiments on polycrystalline San Carlos olivine at up to 5.3 GPa confining pressure and temperatures of 350 to 900^{o}C, which are appropriate to the temperature within a subducting slab (Kincaid & Sacks, 1997). The flow stress of polycrystalline olivine at 500^{o}C and 5 GPa has been estimated at an ultimate strain-rate of ~10^{-7}s^{-1} which is significantly lower than strain rates achieved in previous studies.

Flow Laws

Plastic deformation takes place on an atomic scale by the movement of lattice defects (dislocations) through the crystal (Poirier, 1985, chapter 2). Orowan (1940) proposed that the plastic strain rate ($\dot{\varepsilon}$) is proportional to the dislocation density (ρ) and the average velocity of these dislocations ($\bar{v}$):

$$\dot{\varepsilon} \propto \bar{v}\rho \quad (1),$$

where $\bar{v}$ is a product of the force acting on the dislocation and its mobility (Frost & Ashby, 1982) and ρ is a function of differential stress (σ) with the form (after Argon, 1970):

$$\rho \propto \sigma^{m} \quad (2).$$

The stress dependence, *m*, of the dislocation density has been measured for olivine to be 1.41 ± 0.16 (Karato & Jung, 2003). Since dislocations are not generated or annihilated homogeneously throughout a crystal it takes a finite amount of strain, at a given stress, for the equilibrium dislocation density to be achieved. In a constant stress experiment approximately 3% strain is required for the dislocation density to reach the equilibrium value; at about 1% strain the crystal is within ≈ 85% of the equilibrium dislocation density (Durham *et al.,* 1977). In stress relaxation experiments the equilibrium dislocation density will reduce as the sample deforms. At very low strain rates it is not certain that there will be enough strain on the experimental timescale to reduce the dislocation density to that approaching the equilibrium value. In this case measurement of the dislocation density overestimates the differential

stress.

The mobility of dislocations is controlled by their interaction with obstacles to their motion. The average velocity of dislocations ($\bar{v}$) is a function of the time that they spend overcoming obstacles while passing through a crystal. If the velocity of the dislocations, $\bar{v}$, is determined by the strength and density of discrete obstacles in the crystal, then $\bar{v}$ is given by the kinetic equation (Frost & Ashby, 1982):

$$\bar{v} = K' \exp\left(-\frac{\Delta G(\sigma)}{\mathrm{R}T}\right) \quad (3).$$

In this equation R is the gas constant, T the temperature, K' is a constant and $\Delta G(\sigma)$ is the Gibbs free energy of activation for passing an obstacle. The shape and distribution of the obstacles define $\Delta G(\sigma)$; for short-range obstacles that are sensitive to thermal activation $\Delta G(\sigma)$ has a general form (Kocks *et al.,* 1975):

$$\Delta G(\sigma) = F_0\left[1-\left(\frac{\sigma}{\tau}\right)^p\right]^q \quad (4),$$

where τ is the strength stress at 0 K, F_0 the free energy needed to overcome the obstacle without any external work and p and q take values in the range $0 < p \leq 1$ and $1 \leq q \leq 2$. Ono (1968) concluded that for most values of σ it is sufficiently accurate to take $p = 1/2$ and $q = 3/2$.

If, on the other hand, obstacles to dislocation motion act over a large region of the crystal (long-range obstacles), the form of $\Delta G(\sigma)$ will be (Kocks *et al.*, 1975):

$$\Delta G(\sigma) \propto \ln\left(\frac{\tau}{\sigma}\right) \quad (5).$$

Possible physical mechanisms with an activation energy with this form have been discussed by Seeger (1956) and Schoeck & Seeger (1955) but are beyond the scope of this discussion.

Combining equations 4 and 5 with equations 2 and 3 gives two possible strain-rate equations for short-range and long-range obstacles respectively:

$$\dot{\varepsilon} = A_0\sigma^m \exp\left(\frac{-Q}{\mathrm{RT}}\left[1-\left(\frac{\sigma}{\tau}\right)^p\right]^q\right) \quad (6a),$$

$$\dot{\varepsilon} = A_0\sigma^{m-1} \exp\left(\frac{-Q}{\mathrm{RT}}\right) \quad (6b);$$

where Q is the activation energy per mole and A_0 is a constant of proportionality.

Equation 6a is commonly used to describe flow in the Peierl's regime.

At high temperatures the dependence of strain rate on stress is stronger and the flow law becomes the familiar power-law creep flow law (equation 7) (e.g. Poirier, 1985); in which n is the stress exponent and takes values of between 3 and 10 (Frost & Ashby, 1982).

$$\dot{\varepsilon} = A_0 \sigma^n \exp\left(\frac{-Q}{\mathrm{RT}}\right) \quad (7).$$

For olivines n has been measured to be approximately 3.5 (e.g. Li *et al.* 2004 and references therein). Despite the identical form of equations 6b and 7 it is possible to distinguish between the underlying mechanisms since the value of the stress exponent should be approximately 0.41 for equation 6b (after Karato & Jung, 2003) but greater than ≈3 for equation 7. It is also possible to identify a short-range defect (equation 6a) dependence because a fitted power law stress exponent should be slightly smaller than 1.41, by an amount determined by the stress dependency of the exponential term.

Experimental Methods

Experiments were performed in a belt-type pressure cell in a modified 250-tonne Paris-Edinburgh load frame (Dobson *et al.,* 2005), at a constant end load of 40 tonnes. The apparatus has been designed for stress relaxation experiments on the ENGIN-X instrument at the ISIS spallation neutron facility, Rutherford-Appleton laboratory, UK. The belt has a pre-stressed central cylindrical tungsten carbide core with a 10 mm diameter, 7 mm long cylindrical aperture with 47° conical openings at each end. Natural massive fluorite was used as the gasket material and pressure medium, inside which was a tapered graphite furnace, the olivine sample, and end plugs made from magnesium oxide and tungsten carbide. A thermocouple was run through the furnace across one end of the sample and out through the gaskets. A schematic of the belt design is shown in figure 1. The sample was cored from hot-pressed San Carlos olivine block, with a grain size of between 10 and 100μm grains; it is the same sample as used in the previous study of Dobson *et al.* (2004). The hot pressing was performed at 300 MPa and 900°C for 5 hours, in a nickel jacket.

[insert figure 1 about here]

Several changes were made to the experimental setup of Dobson *et al*. (2005) in order to improve the diffracted signal: (1) the inner pistons were made from tungsten carbide and magnesium oxide, instead of corundum, reducing the number of materials in the diffracting volume; (2) the supporting rings on the tungsten carbide pistons were removed, allowing a larger section of the detector banks to be used which increases the signal to noise ratio. Finally, water cooling has been added to the sides of the belt and the end pistons.

The axisymmetric geometry of the experimental apparatus constrains the radial stress, $\sigma_r = \sigma_2 = \sigma_3$ and the axial stress, $\sigma_a = \sigma_1$ under compression. Therefore measuring the axial and radial elastic strains, ε_a^e and ε_r^e, is sufficient to constrain the stress and strain of the system.

ENGIN-X is a time of flight neutron diffractometer designed for making strain measurements in potentially bulky systems (Santisteban *et al.,* 2006). Two independent detector banks are located at $2\theta = \pm 90^o$ to the incident beam; each has a solid angle coverage of $\pm 15^o$ in both 2θ and ϕ. With this machine geometry, diffraction from lattice planes aligned at $\pm 45^o$ to the incident beam will be observed in the detector banks. Thus if an experiment is performed with the principal stress axis (σ_a) aligned at 45^o to the incident beam, independent measurements of the elastic strains ε_a^e and ε_r^e can be performed simultaneously using the two detector banks.

The total neutron flight path of ENGIN-X is 51.5 metres and lattice spacings can be measured to a precision of tens of microstrains (Santisteban *et al.,* 2006). For this study the d-spacing range collected was 1.03 to 2.75Å.

Each data collection was 20 minutes long; these were then summed into 60 to 100 minute sequential time bins to improve the counting statistics. The diffraction patterns were refined using the Rietveld method implemented in the GSAS suite of programs (Larson & Von Dreele, 2000) with EXPGUI (Toby, 2001) and the resulting cell parameters were then used to calculate the elastic strains. Olivine is orthorhombic and so the strain is not necessarily the same in each crystallographic direction. The Rietveld refinement gives the lattice parameters of the sample measured in the axial and radial directions, as a function of confining pressure, P, temperature, T, and time, t. In this study, the linear elastic strain value in the axial and radial directions was calculated from the volume returned by the Rietveld refinement by:

$$\varepsilon^e = \frac{\sqrt[3]{V_{0,T}} - \sqrt[3]{V_{P,T,t}}}{\sqrt[3]{V_{0,T}}} \quad (8),$$

Here $V_{0,T}$ is the unit cell value measured from the sample in the cell prior to initial compression, which has then been thermally expanded to the temperature of the experiment, and the superscript, *e*, denotes elastic strain. The value for the thermal expansion used in this study was 28.1×10^{-6} (average of the values for fosterite in Fei, 1995).

Assuming that the grains in the olivine sample are randomly orientated, the axial and radial stresses, σ_a and σ_r, are calculated from ε_a^e and ε_r^e by the following relationships (Nye, 1957):

$$\sigma_a = c_{11}\varepsilon_a^e + 2c_{12}\varepsilon_r^e \quad (9a);$$

$$\sigma_r = c_{11}\varepsilon_r^e + c_{12}(\varepsilon_a^e + \varepsilon_r^e) \quad (9b).$$

Where the elastic stiffnesses, c_{ij}, are those of the isotropic aggregate.

The elastic stiffnesses have been measured for single crystals of olivine (Abramson *et al.,* 1997; Isaak, 1992). For randomly orientated polycrystalline aggregates some form of isotropic averaging is needed; we have used the Hill (1952) average of the Voigt (1928) and Reuss (1929) bounds for the polycrystalline average of the single-crystal elastic properties. The room pressure and temperature values and the pressure dependencies of c_{ij} used in this study are taken from Abramson *et al.,* (1997) for $Fo_{92}Fa_8$ and the temperature dependencies are obtained from a linear fit to the $c_{ij}(T)$ of Isaak (1992) for $Fo_{90}Fa_{10}$. These compositions are sufficiently close to that of the present sample ($Fo_{92}Fa_8$) that errors introduced by the compositional dependence of the parameters are not significant. The cross terms between the pressure and temperature dependencies, as well as the non-hydrostatic effects on the elastic modulii, are assumed to be negligible in the pressure and temperature range of the study. The c_{ij} values used are calculated for each temperature at the average confining pressure of all data points at that temperature.

In order to calculate the plastic strain in the system and hence the plastic strain rate the total strain (ε^t) on the system is assumed to remain constant. In order for this to be the case the gaskets and press are assumed to be infinitely stiff, conditions which mean that for a given set of pressure and temperature conditions the experiment is run at constant sample geometry and volume. The total strain in a given direction, *d*, can

be defined as:

$$\varepsilon_d^t = \varepsilon_d^e + \varepsilon_d^p \quad (10),$$

where the superscripts, *t*, *e* and *p*, refer to the total, elastic and plastic strains respectively. The plastic strain cannot be directly measured by diffraction and it results in the sample changing shape at constant stress or, conveniently, a change in elastic strain at constant sample volume and geometry. During plastic deformation of the sample, at a given temperature, the elastic strain, ε^e, is transformed to plastic strain, ε^p. The elastic strain can be divided into components arising from the mean elastic strain, ε_m^e, and the deviatoric elastic strain, ε_Δ^e, and so equation 10 in the axial direction becomes:

$$\varepsilon_a^t = \varepsilon_m^e + \varepsilon_{\Delta a}^e + \varepsilon_a^p \quad (11),$$

where

$$\varepsilon_{\Delta a}^e = \varepsilon_a^e - \varepsilon_m^e \quad (12).$$

Similar equations apply to the radial direction.

For the axisymmetric system employed here, the mean strain, ε_m^e, on the sample is calculated as $(\varepsilon_a^e + 2\varepsilon_r^e)/3$ and if the experiment is run at constant volume this has to remain constant. For stress relaxation at a given pressure and temperature ε_m^e can be measured and if it remains constant it can be assumed that the experimental system is stiff, with ε^t constant. At $t = 0$ the amount of plastic strain is taken to be zero, therefore at $t = 0$ $\varepsilon_a^t = \varepsilon_a^e$. This is schematically presented in figure 2.

[insert figure 2 about here]

If ε_m^e and ε_a^t are constant, differentiating equation 11 with respect to time gives:

$$\frac{d\varepsilon_{\Delta a}^e}{dt} = -\frac{d\varepsilon_a^p}{dt} \quad (13)$$

and so the rate of plastic deformation in the sample can be determined by measuring the changing deviatoric elastic strain with time in the system. The above relations are

true in both the axial and radial directions independently but in the radial direction the deviatoric strain is negative.

The flow laws outlined above (equations 6a, 6b and 7) relate the deviatoric strain rate ($\dot{\varepsilon}^{p}_{\Delta a}$) to the differential stress (σ) and are applicable assuming that the dislocation density approaches the steady-state value. The value of σ may, in turn, be obtained from the strains and the elastic moduli, *via*

$$\sigma = (c_{11} - c_{12})(\varepsilon_a - \varepsilon_r) \quad (14),$$

leading to a set of equations for strain rate in terms of differential strain. If the available data are at closely separated time intervals and show little noise the strain rate may be derived directly from the strains by, for example, fitting a polynomial to the data. In the present experiment the data were not sufficient to allow this approach and so the alternative approach was adopted of integrating the flow laws with respect to time to give strain as a function of time.

The Peierl's stress equation (equation 6a) is not analytically integrable with respect to time and therefore it was numerically integrated. The time steps used were 3 seconds or less; convergence of the fitting solution against time-step was determined by varying the time-step size as an initial iteration of the fitting procedure. The median differential strain in each time step was used to calculate the strain rate at that step by an iterative procedure. This was done for both ε^{e}_{a} and ε^{e}_{r} simultaneously. The Peierl's stress parameters and the starting strains, $\varepsilon^{e}_{a,t=0}$ and $\varepsilon^{e}_{r,t=0}$, were then optimized to the experimental data. For the sake of consistency the same technique was also employed for fitting equations 6b and 7 as well as analytically integrating; both methods gave the same results to within one standard error.

To investigate the long term strength of olivine the 500°C experiment was run for 96.5 hours. At the end of the experiment σ was barely resolvable by neutron diffraction measurements so we used the dislocation density of the recovered sample as a proxy for the differential stress in the sample at the time the experiment was quenched. The dislocation density was measured using a JEOL JSM6480 LV scanning electron microscope (SEM) after decoration of the sample in a furnace at 900°C in air for an hour, following the method of Kohlstedt & Vander Sande (1975). For the imaging, a 3.5k magnification was used in back-scattered mode. The accelerating voltage was 20kV and the beam current was ≈700nA. Oxidation of the

253 dislocations results in lines of higher back-scattering intensity in the SEM images;
254 these were counted and their density determined. The differential stress was then
255 calculated from equation 2, with m = 1.41 ± 0.16 and a constant of proportionality of
256 $10^{9.04 \pm 0.41}$ (Karato & Jung, 2003) and assuming there is negligible change in the
257 length of the Burgers vector between room pressure and temperature and 5 GPa,
258 500°C.

259 The unit cell measurements were made over two experimental runs: the first
260 experiment was at 350 and 500°C after which the sample was recovered for
261 microanalysis; the second experiment was run at 730 and 900°C. For each experiment
262 the unit cell values were measured from the sample in the open press, at pressure but
263 before heating, and then during stress relaxation. Measurements of the heated sample
264 were started immediately upon arriving at the desired temperature. The experimental
265 runs at 730 and 900°C are short because of technical difficulties with the experimental
266 equipment but we do not think that this impacts on the results of the experiments.
267
268 **Results**
269 A typical diffraction pattern, collected at 500°C, is presented in figure 3; the
270 collection time was approximately 60 minutes. The data have been fitted by
271 diffraction peaks for olivine, MgO and fluorite, along with a background, using the
272 Rietveld refinement method; with this collection time strains of $\approx 5 \times 10^{-4}$ can be
273 resolved.
274
275 [insert figure 3 about here]
276
277 Linear strains calculated from the diffraction data (equation 8) are presented in
278 figure 4 and table 1; for completeness, the V_0 values are also included in table 1. At
279 350°C ε_r^e is approximately constant for the duration of the experiment, suggesting
280 that the constant volume and geometry assumptions are not valid; this is probably due
281 to the gaskets flowing. At 500°C and above the data show approximately constant ε_m^e.
282 At 350 and 730°C the points at $t = 0$ have been calculated from the room temperature
283 data, assuming constant sample geometry and instantaneous heating. It is possible to
284 do this because a new experiment was started between the 500°C and 730°C runs. The
285 mean stresses calculated from the diffraction data and elastic constants for these

pressure and temperature conditions are given in table 2.

[insert table 1 about here]

[insert figures 4a, b, c and d about here]

[insert table 2 about here]

It is not known *a priori* which of the flow laws will best describe the behaviour of olivine at each temperature and so firstly the power law (equation 7) was fitted to the data by the numerical integration method. If $n < 3$ then the low temperature laws (equations 6a and 6b) were then fitted to the data using values of $m = 1.41$ (after Karato & Jung, 2003), with $p = 1/2$, $q = 2/3$ (Ono, 1968) where needed.

Equation 7 gives values for n of 0.46 and 0.54 for the data at 350 and 500°C respectively with R^2 values of 0.987 and 0.973. These exponents are much less than 3 and closer to the value of the stress exponent expected for equation 6b. It is not possible to determine accurate values of the parameters from equation 7 for the 730 and 900°C data because the sample relaxation was faster than the time resolution of the experimental method.

For the 500°C data, minimising the sum of the squares of the misfits for equation 6a results in unreasonably large values for τ (greater than 10^{10} GPa) and $R^2 = 0.949$; the very high, physically unreasonable, value for τ has the effect of making the exponential term independent of stress. Conversely, fitting the data to the long-range obstacle law (equation 6b) is more sensible because the fit is consistent with the observed stress dependence and does not produce any physically unreasonable values. The fits to the 500°C data for the short-range and long-range obstacle laws are presented in figure 5; their coefficients are given in table 3 together with the coefficients from equation 7 (the power law), which are included for comparison.

If this fitting is also performed on the 350°C data, assuming that the constant

volume and geometry assumptions are valid, equation 6b (R^2 = 0.987; constant of proportionality = 3.1 × $10^{-7}s^{-1}GPa^{-0.41}$) also fits the data better than equation 6a (R^2 = 0.974). Fitting the power law equation (7) to the data the optimum value for the stress exponent is 0.46 (R^2 = 0.987; constant of proportionality of 3.2 × $10^{-7}s^{-1}GPa^{-0.46}$), which is consistent with the *m-1* value of equation 6b given the stress dependence of dislocation density determined from Karato & Jung (2003).

[Insert figure 5 about here]

[insert table 3 about here]

From the recovered sample that had undergone stress relaxation for 4 days (96.5 hours) at 500°C, 1236 μm length of straight dislocations were measured from 2935 μm^2 of suitable images. This corresponds to a differential stress of 68 +180/-44 MPa in equilibrium with this dislocation density (see above); the error was estimated by assuming a factor of two error because of uncertainty in the penetration depth of the electron beam and some indistinctiveness of the image's oxidised dislocation lines. According to the fitted flow law (6b) this differential stress is reached in a time of 34.8 +3.5/-7.1 × 10^3 seconds, i.e. approximately 10 hours, and at this time the strain rate is calculated to be 7.2 +7.0/-3.1 × $10^{-8}s^{-1}$. Given that the stress then appears not to change over the next 87 hours of relaxation, we consider 68 +180/-44 MPa to be the yield stress of the sample. However, since we have performed stress relaxation experiments and the amount of strain in the sample was <3%, this estimate, based on the dislocation density in the sample, provides an upper limit on the yield stress.

If, however, the differential stress measured from the recovered sample is assumed to be the differential stress just before the experiment was completed, a lower limit for the strain rate can be estimated. By assuming the strain rate is constant between the time of the last diffraction measurement and the recovery of the sample, as well as constant pressure, the lower limit for the strain rate is 1.9 +9.9/-9.5 × $10^{-9}s^{-1}$. Perhaps obviously, if the fitted flow law was extrapolated to the same time the estimated strain rate would be approximatly another order of magnitude lower.

The 730°C data show a significant difference from the lower temperature data in

that the differential strain has reduced to a barely resolvable level within the first 360 seconds of the experiment, which is much faster than the time of approximately 2×10^4 seconds taken at 350°C and 500°C. This cannot be said to be because there was no starting differential strain because (a) the differential strain was measured to be $10.5 \pm 0.1 \times 10^{-3}$ at room temperature and high pressure before the 730°C experiment and (b) heating increases the differential strain. This can be seen by comparing the values of differential strain measured immediately before and after changing the temperature (see figures 4a and b). Similarly, the differential strain generated by the experiment upon heating to 900°C has annealed out completely within the first 600 seconds of the experiment. Therefore, at 730°C and above, the olivine is much weaker than at below 500°C, but whether the flow law is a short-range obstacle law (equation 6a) or a power law type (equation 7) cannot be determined in the present study.

Discussion

The model which best fits the 350 and 500°C data has a long-range obstacle resistance to the motion of the dislocations in which $\Delta G(\sigma)$ has the form presented in equation 5 (Kocks *et al.*, 1975). This is not related to the build up of immovable dislocation tangles and indeed none of these were observed during the SEM analysis of the decorated samples.

Between 500 and 730°C the deformation mechanism changes from a long-range obstacle mechanism to one that allows for faster deformation; whether this is a short-range defect law (equation 6a) or a power law creep (equation 7) cannot be determined from the results presented here. A change in mechanism between 500 and 730°C is consistent with the results of Ratteron *et al*. (2004), Li *et al.* (2006) and Yamamoto *et al.* (2008) who see weakening in olivine at temperatures between 500 and 600°C. The good agreement between the present results and those of previous studies, which were performed at significantly higher strain rates, suggest that the temperature of weakening in olivine flow stress is not strongly dependent on strain-rate, allowing us to extend the present observations to the Earth.

The upper limit for the long term yield stress of olivine determined here at 500°C is 68 +180/-44 MPa; at 730°C and starting from a differential stress of 1.53GPa the stress relaxed to a value which was below the detection limit of the technique employed here within 360 seconds. The 500°C value of the yield stress determined

here is close to maximum estimates of the stress drop during intermediate earthquakes (~40 MPa at 100 km; Venkataraman and Kanamori, 2004). This suggests that the weakening observed here, and in other studies, at temperatures between 500 and ~700°C will cause the plastic yield strength of olivine to drop below its brittle failure strength, resulting in a cessation of seismicity. McKenzie *et al.* (2005) report that, in oceanic crust, "most earthquakes occur in crustal or mantle material that is cooler than 600°C". Similarly, Frohlich, (2006) found that the cessation of intermediate seismicity corresponds closely with the 800°C isotherm in subducting slabs. Furthermore, the maximum elastic thicknesses of the oceanic crust reported by Watts (2001) correspond with the 600°C isotherm of McKenzie *et al.* (2005). All of these observations are consistent with the weakening of olivine between 500–730°C determined here and, further support our contention that this observed weakening is largely independent of strain-rate.

Acknowledgements

Simon Hunt is grateful for his NERC scholarship; David Dobson gratefully acknowledges his Royal Society URF and EU support as part of the Marie Curie Research Training Network, C2C. The authors would like to thank Steve Boon and Jim Davy for technical assistance. ISIS experiment number: RB100042. The authors thank C. Marone and one anonymous reviewer for helpful comments that aided improvements to the manuscript.

References

Abramson, E.H., Brown, J.M., Slutsky, L.J., Zuag, J., 1997, The elastic constants of San Carlos olivine to 17 GPa. J. Geophys. Res., 102: 12253 – 12263.

Argon, S.A., 1970, Internal stresses arising from the interaction of mobile dislocations. Scripta Metall., 4: 1001 –1004.

Bina, C.R., Wood, B.J., 1986, The 400-km seismic discontinuity and the proportion of olivine in the Earth's upper mantle. Nature, 324: 449 – 451.

Dobson, D.P., Meredith, P.G., Boon, S.A., 2004, Detection and analysis of microseismicity in multi anvil experiments. Phys. Earth Planet. Inter., 143 – 144: 337 – 346.

417 Dobson, D.P., Mecklenburgh, J., Alfe, D., Wood, I.G., Daymond, M.R., 2005, A new
418 belt-type apparatus for neutron-based rheological measurements at Gigapascal
419 pressures. High Pressure Research, 25: 107 – 118.
420 Durham, B., Goetze, C., Blake, B., 1977, Plastic flow of oriented single crystals of
421 olivine: 2. Observations and interpretations of the dislocation structures. J.
422 Geophys. Res., 82: 5755 – 5770.
423 Evans, B., Goetze, C., 1979, Temperature-variation of hardness of olivine and its
424 implication for polycrystalline yield stress. J. Geophys. Res., 84: 5505 – 5524.
425 Fei, Y., 1995, Thermal expansion in: Ahrens, J. T. (editor) Mineral Physics &
426 Crystallography: A Handbook of Physical Constants (Agu Reference Shelf, No 2),
427 29 – 44.
428 Freed, A., Bürgmann, R., 2004, Evidence of power-law flow in the Mojave desert
429 mantle. Nature, 430: 548 – 550.
430 Frolich, C., 1989, The nature of deep-focus earthquakes. Ann. Rev. Earth Planet. Sci.
431 17: 227 – 254.
432 Frohlich, C., 2006, A simple analytical method to calculate the thermal parameter and
433 temperature within subducted lithosphere. Phys. Earth. Planet. Inter., 155, 281-285.
434 Frost, H.J., Ashby, M.F., 1982, Deformation-mechanism maps: The plasticity and
435 creep of metals and ceramics. Pergamon Press, Oxford, 175 pp.
436 Green, H. W., Borch, R. S., 1987, The Pressure-Dependence of Creep. Acta Metall.,
437 35: 1301–1305.
438 Hill, R., 1952, The elastic behaviour of a crystalline aggregate. Proc. Phys. Soc., A,
439 65: 349 – 354.
440 Isaak, D.G., 1992, High-temperature elasticity of iron-bearing olivines. J. Geophys.
441 Res., 97: 1871 – 1885.
442 Kanamori, H., & Anderson, D.L., 1975, Theoretical basis of some empirical relations
443 in seismology. Bull. Seismol. Soc. Am., 65: 1073–1095.
444 Karato, S.I., Jung, H., 2003, Effects of pressure on high-temperature dislocation creep
445 in olivine. Phil. Mag., 83: 1478-6435.
446 Kincaid, C., Sacks, I.S., 1997, Thermal and dynamical evolution of the upper mantle
447 in subduction zones. J. Geophys. Res., 102: 12295 – 12316.
448 Kocks, U.F., Argon, A.S., Ashby, M. F., 1975, Thermodynamics and the kinetics of
449 slip in: Progress in Materials Science, vol. 19, Pergamon Press, Oxford, 300 pp.

Kohlstedt, D.L., Vander Sande, J.B., 1975, An electron microscopy study of naturally occurring oxidation produced precipitates in iron-bearing olivines. Contrib. Mineral. Pet., 53: 13 – 24.

Larson, A.C., Von Dreele, R.B., 2000, General Structure Analysis System (GSAS). Los Alamos National Laboratory Report LAUR 86-748.

Li, L., Weider, D.J., Raterron, P., Chen, J., Vaughan, M., 2004,. Stress measurements of deforming olivine at high pressure. Phys. Earth Planet. Inter., 143 – 144: 357 – 367.

McKenzie, D., Jackson, J., Priestley, K., 2005, Thermal structure of oceanic and continental lithosphere, Earth Planet. Sci. Lett., 233: 337 – 349.

Nye, J.F., 1957, Physical properties of crystals: their representation by tensors and matrices. Oxford University press, Oxford, 352 pp.

Ono, K., 1968, Temperature dependence of dispersed barrier hardening. J. Appl. Phys., 39: 1803 – 1806.

Orowan, E., 1940, Problems of plastic gliding. Proc. Phys. Soc., 52: 8 – 22.

Poirier, J-P., 1985, Creep of Crystals: High-Temperature Deformation Processes in Metals, Ceramics and Minerals. Cambridge University Press, Cambridge, 274 pp.

Raterron, P., Wu, Y., Weider, D.J., Chen, J., 2004, Low-temperature olivine rheology at high pressure. Phys. Earth Planet. Inter., 145: 149 – 159.

Reuss, A., 1929, Berechnung der fliessgrenze von mischkristallen auf grund der plastizitatsbedingung fur einkristalle. Zeitschrift fur Angewandte Mathematik und Mechanik, 9: 49 – 58.

Ross, J.V., Ave'Lallemant, H.G., Carter, N.L., 1979, Activation volume for creep in the upper mantle. Science, 203: 261 – 263.

Santisteban, J.R., Daymond, M.R., James, J.A., Edwards, L., 2006, ENGIN-X: a third-generation neutron strain scanner. J. Appl. Crystal., 39: 812–825.

Schoeck, G., Seeger, A., 1955, Report of conference on defects in crystalline solids, p. 340 London physical society.

Scott Blair, G.W., 1933, On the nature of 'yield-value'. J. Appl. Phys., 4: 113 – 118.

Seeger, A., 1956, On the theory of the low-temperature internal friction peak observed in metals. Phil. Mag., 1: 651 – 662.

Toby, B.H., 2001, EXPGUI, a graphical user interface for GSAS. J. Appl. Crystall., 34: 210 – 213.

Venkataraman, A., Kanamori, H., 2004, Observational constraints on the fracture energy of subduction zone earthquakes. J. Geophys. Res., 109: B05302.

Voigt, W., 1928, Lehrbuch der Kristallphysik. Teubner, Leipzig.

Watts, A. 2001, Isostacy and flexure of the lithosphere, Cambridge University Press, Cambridge, 458pp

Yamamoto, J., Ando, J., Kagi, H., Inoue, T., Yamada, A., Yamazaki, D., Irifune, T., 2008, In situ strength measurements on natural upper-mantle minerals, Phys. Chem. Minerals, DOI 10.1007/s00269-008-0218-6

FIGURE CAPTIONS

Figure 1. Diagram of the cell design, belt and pistons. The section illustrated is a vertical section and so the thermocouple is out of the plane of the incident and diffracted beams. Excluding the thermocouple, the dot-dash line is the rotation axis of the experimental setup. This line is also where the plane of the incident and diffracted beams intersect the figure.

Figure 2. Illustrative figure showing how ε_{Δ}^{e} and ε^{p} evolve with time during the experiment. The solid curves are the directly observable values and the various dashed lines show quantities derived from them.

Figure 3. Typical diffraction pattern collected over one hour from the beginning of the 500°C data set. The upper trace is the Rietveld refinement of the data (the points showing the observations and the line showing the calculated diffraction pattern) and the lower trace is the difference plot. The ticks correspond to positions of reflections of (from top to bottom) fluorite, MgO and olivine.

Figure 4. Plots of strain against time for olivine. Filled circles are ε_{a}^{e} and open circles are ε_{r}^{e}; the error bars shown are plus and minus two standard deviations from the Rietveld fit. The squares in the 350 and 730°C data denote the $V_{0,T}$ for each of the experiments. Note the different time scale for (c) and the change in both scales for (d).

Figure 5. Plot of $\varepsilon_{\Delta a}^{e}$ (filled circles) and $\varepsilon_{\Delta r}^{e}$ (open circles) against time; in this plot $\varepsilon_{m}^{e} = 0$. The solid lines are the fits from equation 6a and the dashed lines from equation 6b. The error bars are two standard deviations as returned by the Rietveld refinements.

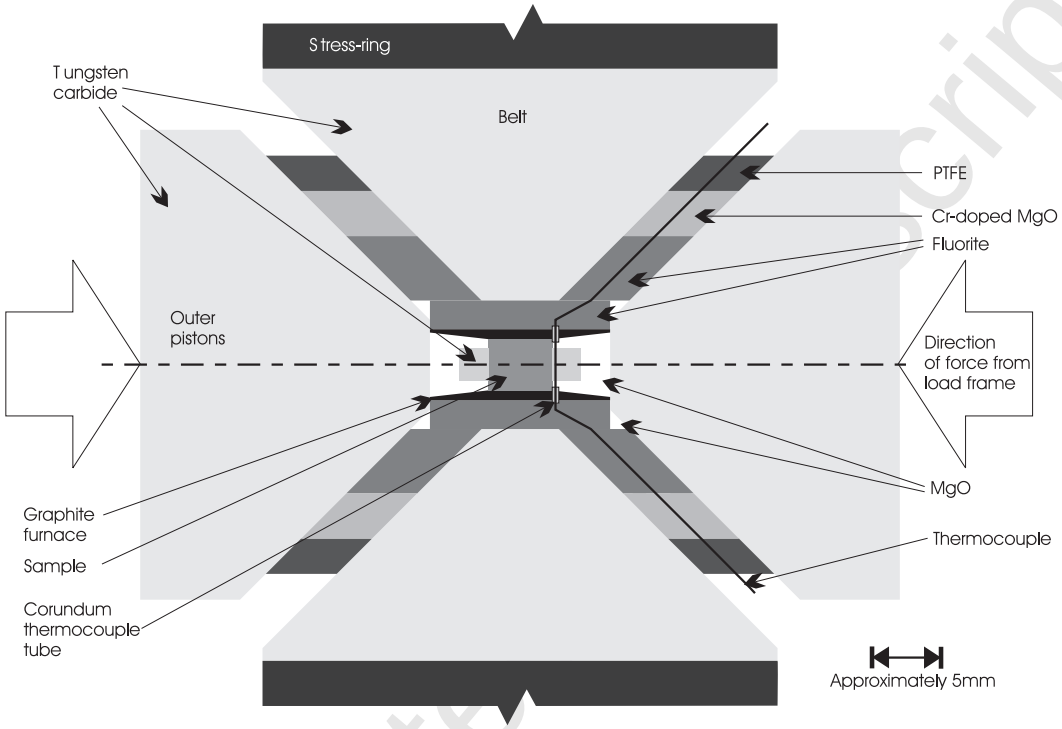

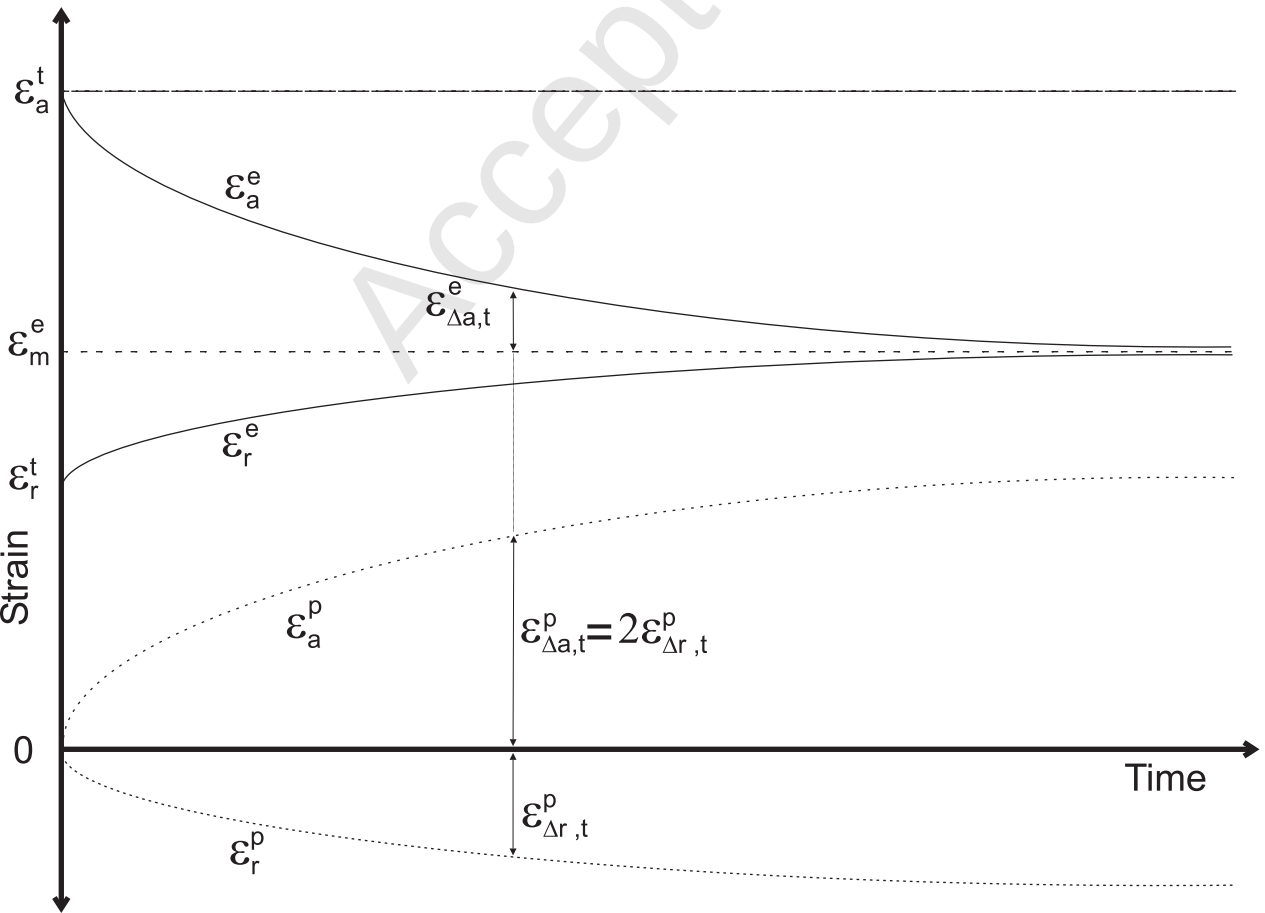

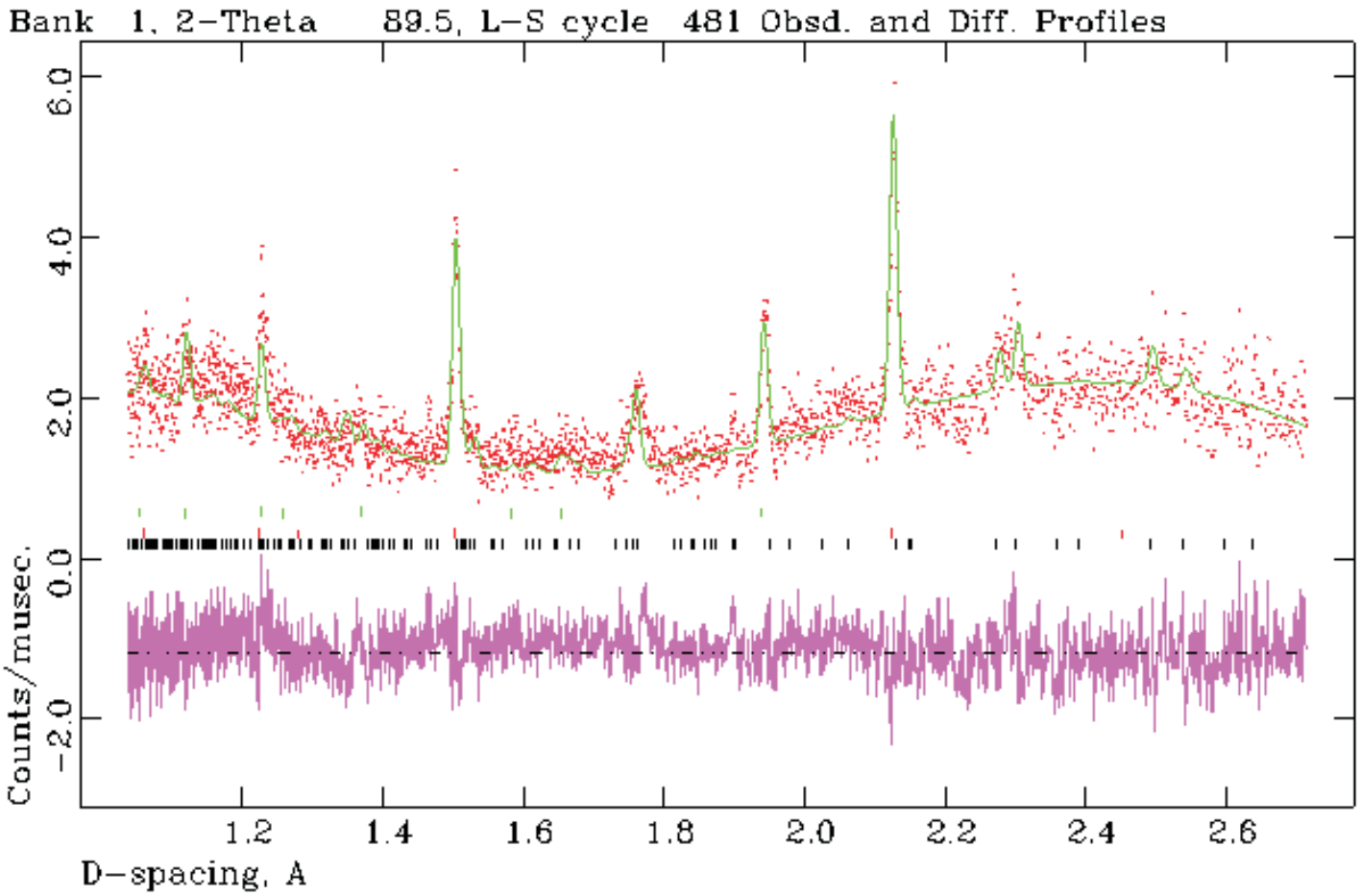

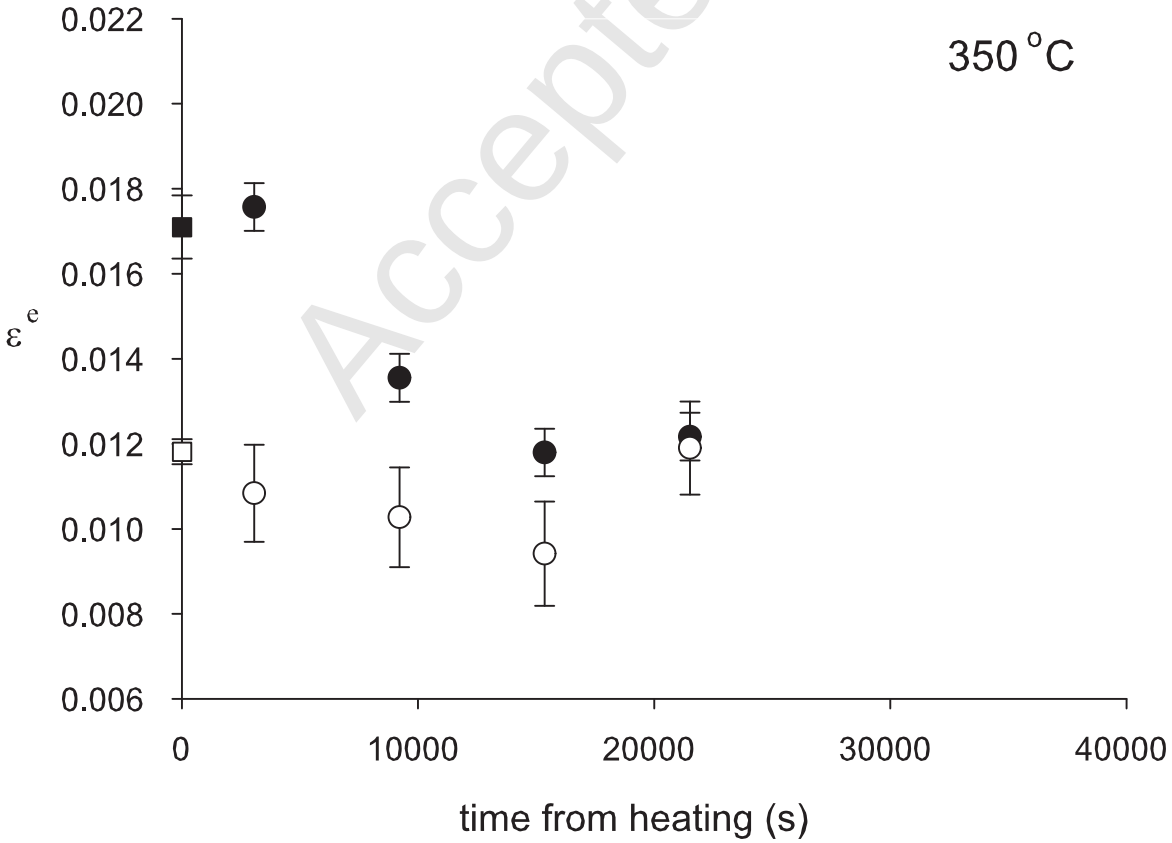

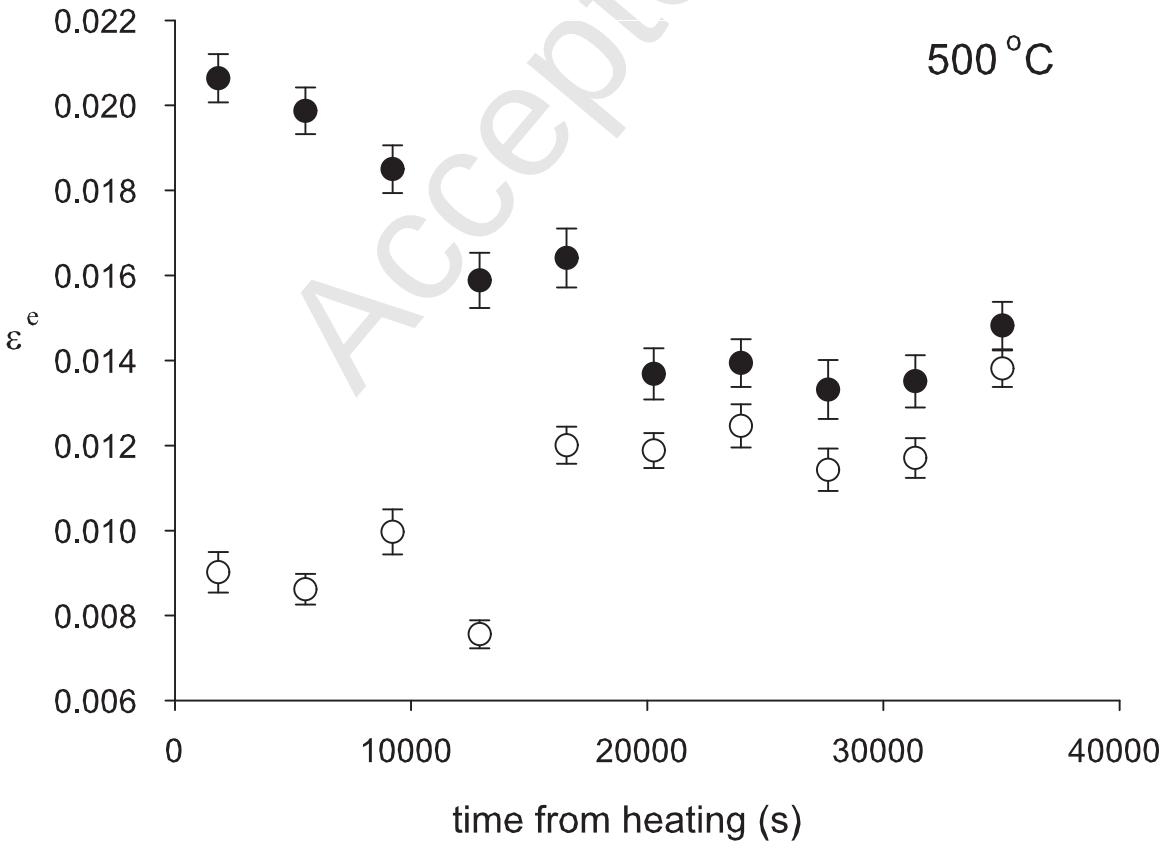

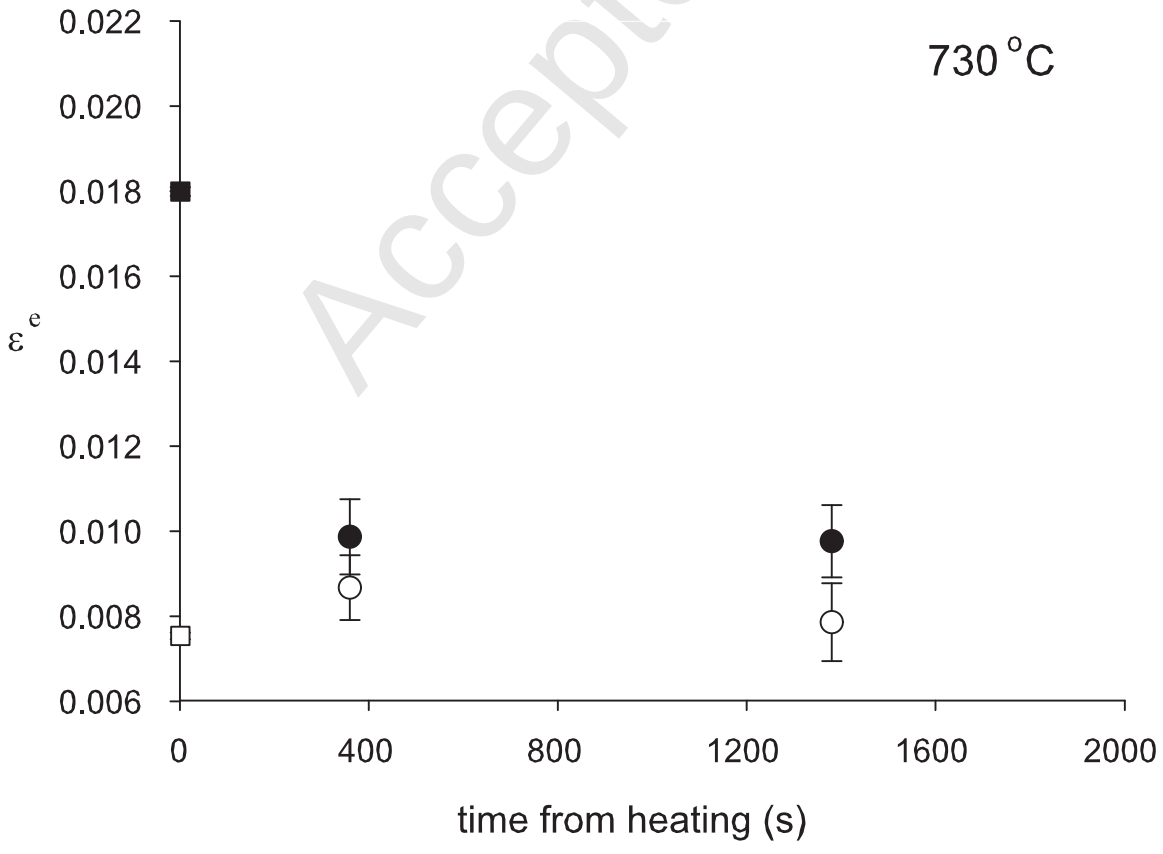

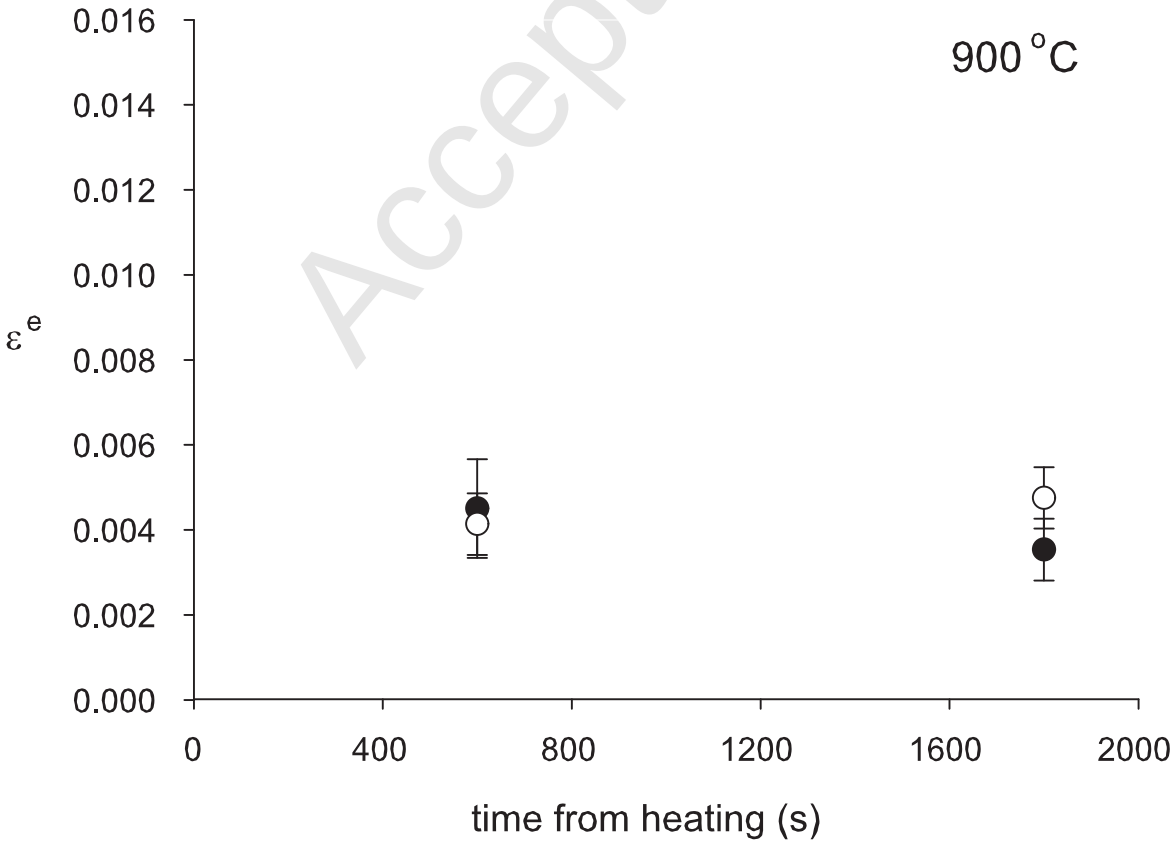

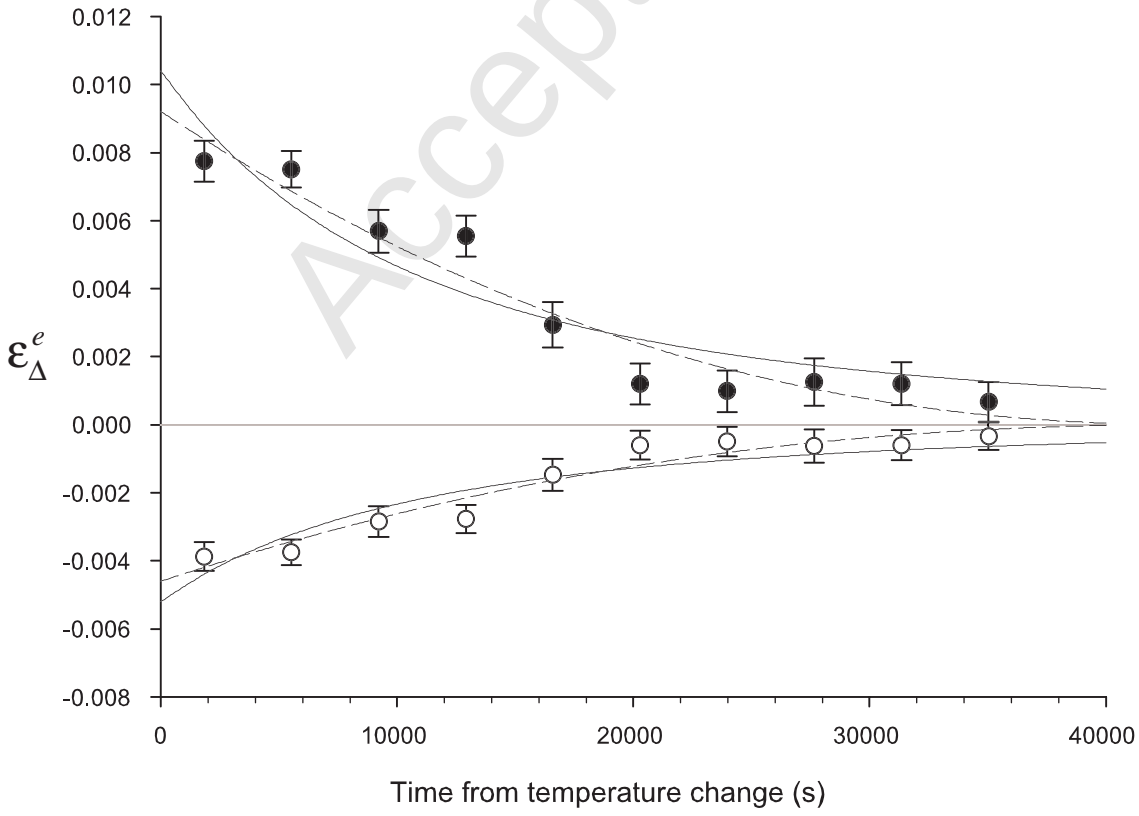

Temperature (^{o}C)	Time (s)	ε_a^e	ε_r^e
350	0	0.0171(4)	0.0118(3)
[$V_{0,a}$ = 297.75 ± 0.22 Å^3]	3060	0.0176(3)	0.0108(6)
[$V_{0,r}$ = 293.01 ± 0.07 Å^3]	9210	0.0136(3)	0.0103(6)
	15360	0.0118(3)	0.0094(6)
	21510	0.0122(3)	0.0119(5)
500	1830	0.0206(3)	0.0090(2)
	5520	0.0199(3)	0.0086(2)
	9210	0.0185(3)	0.0100(2)
	12900	0.0159(3)	0.0076(2)
	16590	0.0164(3)	0.0120(2)
	20280	0.0137(3)	0.0119(2)
	23970	0.0139(3)	0.0125(2)
	27660	0.0133(3)	0.0114(2)
	31350	0.0135(3)	0.0117(2)
	35040	0.0148(3)	0.0138(2)
730	0	0.0180(1)	0.0075(1)
[$V_{0,a}$ = 291.42 ± 0.04 Å^3]	360	0.0099(4)	0.0087(4)
[$V_{0,r}$ = 291.89 ± 0.04 Å^3]	1380	0.0098(4)	0.0079(5)
900	600	0.0045(6)	0.0041(4)
	1800	0.0035(4)	0.0048(4)

Table 1. Table containing the strains calculated from the diffraction data as well as the measured V_0 values for each experiment. The numbers in brackets are one standard error to the fit in the last decimal place.

Temperature (^{o}C)	c_{11} (GPa)	c_{12} (GPa)	Confining pressure (GPa)
350	252.06	90.82	5.0 ± 0.5
500	248.57	90.52	5.3 ± 0.4
730	227.78	81.71	3.3 ± 0.2
900	209.54	73.81	1.3 ± 0.2

Table 2. Converged elastic constants, confining pressures used to calculate the stress relaxation curves at each temperature.

Variable	Short-range obstacles	Long-range obstacles	'Power law'
$\varepsilon^{e}_{\Delta a,0}$	**0.0104**	**0.0092**	**0.0092**
Constant of proportionality	**3.5×10^{-7}**	**3.1×10^{-7}**	**3.0×10^{-7}**
Stress exponent (*m*, *m-1* or *n*)	1.41*	0.41*	**0.54**
R^2	**0.949**	**0.972**	**0.973**

Table 3. Table showing the coefficients calculated for the short-range obstacle (equation 6a), long-range obstacle (equation 6b) and power law (equation 7) flow laws for the 500°C data. The numbers marked by an asterisk were fixed in the analysis. The units of the constant of proportionality are s^{-1} GPa^{-r} where r = *m, m-1 or n* as required.